



1 Perchloric acid (HClO₄) Drives Atmospheric New
2 Particle Formation Enhanced by Dimethylamine,
3 ammonia and Sulfuric Acid: Mechanisms and
4 Implications

5
6 Shengming Wang^{2,3}, Xiangli Shi^{1,*}, Qingzhu Zhang², Wenxing Wang²,

7
8
9 ¹College of Geography and Environment, Shandong Normal
10 University, Jinan 250014, P. R. China

11 ²Environment Research Institute, Shandong University,
12 Qingdao 266237, P. R. China

13 ³Laboratory of Atmospheric Environment and Pollution Control,
14 Research Center for Eco-Environmental Sciences, Chinese Academy of
15 Sciences, Beijing 100085, China

16
17
18 **Keywords:** New particle formation, Perchloric acid, Marine aerosol,
19 Particle formation rate, Cluster concentration, Atmospheric nucleation
20 precursor

21
22 *Corresponding authors. E-mail: shixl@sdnu.edu.cn



23

Abstract

24

25 Recent studies have revealed observations of atmospheric perchloric acid
26 (HClO₄, PA) in the Arctic. There are few studies of PA forming aerosol particles in
27 coastal marine regions. We use quantum chemical calculations and Atmospheric
28 Clusters Dynamic Code (ACDC) to compare the enhancement potential of
29 dimethylamine (DMA), ammonia (NH₃), and sulfuric acid (SA) for PA-based new
30 particle formation (NPF). The results show that DMA and NH₃ can strongly interact
31 with PA in both directions through hydrogen bonding and proton transfer. Halogen
32 bonding is not found in PA-DMA and PA-NH₃ clusters. Even if the concentration of
33 NH₃ exceeds that of DMA by 10-100 orders of magnitude, the cluster formation rate
34 of PA-DMA cluster formation is much higher than that of the PA-NH₃ cluster system.
35 Clusters with the same number of PA molecules as DMA molecules play a key role in
36 the growth of PA-DMA clusters. Compared with the nucleation of PA with SA, PA
37 nucleates more easily with alkaline gas. The present results reveal the potential for
38 new particle formation of PA in the Arctic boundary layer.

39

40

41

42



43

44 **1 Introduction**

45

46 At least 50% of the overall concentration of aerosol particles in the atmosphere is
47 believed to be attributed to new particle formation (NPF) (Ehn et al., 2014). Because
48 they reflect and absorb solar radiation, reduce visibility, and have an indirect and
49 direct impact on the climate, these aerosols have a deleterious impact on human
50 health (Zhang, 2010). The production mechanism and subsequent expansion of aerosol
51 particles are poorly understood, making them one of the biggest uncertainties in
52 global climate models (Masson-Delmotte et al., 2021). Theoretical studies, laboratory
53 experiments, and field measurements of air aerosols and nucleation events are
54 available (Lee et al., 2019; Chu et al., 2019; Kalivitis et al., 2019). The nucleation of
55 amines and ammonia in the atmosphere using sulfuric acid (SA) is a crucial process in
56 the contaminated boundary layer (Chen et al., 2012; Erupe et al., 2011; Jen et al.,
57 2014; Loukonen et al., 2010; Zhao et al., 2010; Zollner et al., 2012). Nevertheless, SA
58 concentrations in the atmosphere are typically too low to support cluster growth to
59 CCN size. The particle production and subsequent growth stages are significantly
60 influenced by other nucleating agent candidates in the atmosphere.

61 NPF can occur through a variety of nucleation pathways and involves important
62 precursors like sulfuric acid (H_2SO_4), iodine oxoacids (HIO_x , HIO_2 , and HIO_3),
63 low-volatility organic compounds, ammonia (NH_3), and amines, as shown by
64 laboratory experiments and theoretical calculations (He et al., 2023; He et al., 2021;



65 Kirkby et al., 2023). By discovering significant perchlorate (ClO_4^-), recent
66 investigations have conjectured the possible formation of perchloric acid (HClO_4 , PA)
67 in the lower atmosphere (Dasgupta et al., 2005; Rajagopalan et al., 2009; Furdui and
68 Tomassini, 2010; Barrie et al., 1988). Atmospheric PA, the sinking process of
69 chlorine, was initially identified as a significant component in the polar stratosphere
70 (Sander et al., 1989; Webster et al., 1993; Jaeglé et al., 1996). Tham et al. shown the
71 presence of PA in the Arctic region, an atmospheric sink for reactive chlorine that has
72 not been previously considered (Tham et al., 2023). The observed concentration
73 ranges of PA is 3×10^4 - $1 \times 10^6 \text{ cm}^{-1}$ in the Arctic atmosphere(Tham et al., 2023).
74 Previous studies have found that chloric acid makes a relatively small contribution to
75 new particle formation(Wang et al., 2025). Perchloric acid is a major component of
76 chloric acid, and its contribution to new particle formation requires further
77 investigation. The most prevalent and powerful organic base in the environment is
78 dimethylamine (DMA), which significantly accelerates ion-induced and neutral
79 SA-water nucleation (Ge et al., 2011; Jen et al., 2014). The concentration of DMA
80 surpasses 3 parts per trillion by volume, according to experiments, and the nucleation
81 rates of DMA are significantly higher than those of ambient ammonia (Almeida et al.,
82 2013).

83 In this paper, the nucleation mechanism of $(\text{PA})_{1-4}(\text{DMA})_{1-4}$, $(\text{PA})_{1-4}(\text{NH}_3)_{1-4}$,
84 and $(\text{PA})_{1-4}(\text{SA})_{1-4}$ systems are investigated using quantum chemical calculations and
85 the Atmospheric Clusters Dynamic Code (ACDC) methods. Furthermore, the
86 relationships between various components and the thermodynamic characteristics of



87 PA-related clusters were examined. Lastly, ACDC used dynamic simulations to
88 examine the evaporation rates, formation paths, dimer concentrations, and particle
89 formation rates of PA-related clusters using thermodynamic data from three
90 PA-DMA, PA-NH₃, and PA-SA systems.

91

92 **2 Computational methods**

93

94 To find the global minimum of the (PA)₁₋₄(DMA)₁₋₄, (PA)₁₋₄(NH₃)₁₋₄ and
95 (PA)₁₋₄(SA)₁₋₄ clusters, we used a multi-step global minimum sampling approach. the
96 ABCluster software was employed to randomly construct the initial structures of 1000
97 - 10,000 (PA)₁₋₄(DMA)₁₋₄, (PA)₁₋₄(NH₃)₁₋₄ and (PA)₁₋₄(SA)₁₋₄ clusters(Zhang and
98 Dolg, 2015). In addition, the Universal force field (UFF) (Rappé et al., 1992) was
99 used to describe every molecule in the ABCluster software (Zhang and Dolg, 2015).
100 Initially, from structures (>20,00) produced by the artificial bee colony algorithm
101 (Karaboga, 2005) for cluster (ABCluster), 1000 structures with comparatively low
102 energy were selected. In the multistep sampling scheme, the geometry optimization is
103 carried out at the PM7, ωB97X-D/6-31+G(d,p) and ωB97X-D/6-31++G(d,p) levels of
104 theory, and the single-point energy calculations are executed at the
105 DLPNO-CCSD(T)/aug-cc-pVTZ level of theory based on the ωB97X-D/6-31++G(d,p)
106 theory level. The PM7 and ωB97X-D computations were carried out utilizing the
107 GAUSSIAN 09 program package(Frisch et al., 2016). ORCA 4.0.0 was implemented
108 to perform DLPNO-CCSD(T) computations(Neese, 2012). The initial structures will



109 be modified and re-optimized until the optimization is successful in order to address
110 convergence issues and failures, such as terminating with a false frequency in the
111 optimization of the $(PA)_{1-4}(DMA)_{1-4}$, $(PA)_{1-4}(NH_3)_{1-4}$ and $(PA)_{1-4}(SA)_{1-4}$ cluster
112 geometries. PA-DMA clusters' free energy of formation (ΔG) is computed at various
113 temperatures (238, 258, and 278 K). The structures of $(SA)_{1-4}$, $(NH_3)_{1-4}$ and
114 $(DMA)_{1-4}$ clusters were obtained from previous studies and are recalculated here(Xie
115 et al., 2017; Ge et al., 2011; Jen et al., 2014; Almeida et al., 2013).

116

117 **Atmospheric Cluster Dynamics Code (ACDC) Simulation**

118 ACDC was applied to compute the growth pathway, steady-state concentrations,
119 and time-evolving cluster formation rates for the $(PA)_{1-4}(DMA)_{1-4}$, $(PA)_{1-4}(NH_3)_{1-4}$
120 and $(PA)_{1-4}(SA)_{1-4}$ clusters(Mcgrath et al., 2012a; Mcgrath et al., 2012b). The results
121 of the experiments employing the birth and death equations and the conclusions of the
122 ACDC simulations correspond well(Mcgrath et al., 2012b). In this study, ACDC
123 simulations were performed to model the formation process of PA-DMA, PA-NH₃
124 and PA-SA neutral clusters without considering the effects of charge and
125 water(Mcgrath et al., 2012b). For the studied PA-DMA clusters, the $\beta_{DMA}C_{DMA}/\Sigma\gamma$ of
126 $(PA)_5(DMA)_5$ cluster is greater than 1. According to the ACDC manual(Mcgrath et al.,
127 2012b), a system size of 6 molecules is large enough. The resulting PA-DMA systems
128 $(PA)_5(DMA)_5$ cluster is set as boundary clusters. The concentration ranges of [PA],
129 [SA], [DMA] and [NH₃] were defined at $10^6 - 10^8 \text{ cm}^{-3}$, $10^6 - 10^8 \text{ cm}^{-3}$, 0.1–100 ppt
130 and 1–100 ppt, respectively(Xie et al., 2017; Ge et al., 2011; Jen et al., 2014; Almeida



131 et al., 2013).

132

133 **3 Results and discussion**

134

135 3.1 Cluster structures and cluster formation free energy

136 Figure 1 displays the $(\text{PA})_{1-4}(\text{DMA})_{1-4}$ clusters identified minimum free energy
137 configurations at the DLPNO-CCSD(T)/aug-cc-pVTZ// ω B97X-D/6-31++G(d,p) level
138 of theory. Proton transfer and hydrogen bonding stabilize the majority of PA–DMA
139 clusters. The formation of halogen bond is not found in PA–DMA clusters. All
140 PA–DMA heteromolecular clusters have been discovered to undergo proton transfer,
141 in which the hydrogen atom of hydroxyl group in the PA molecule moves to the
142 nitrogen atom of the NH_2^- group in the DMA to produce N–H...Cl–O hydrogen bond.
143 Each PA molecule donates a proton to a DMA molecule when the quantity of PA
144 molecules and DMA molecules is equal.

145 When the number of PA molecules is not equal to the number of DMA molecules,
146 the number of proton transfers between PA and DMA depends on the smaller value of
147 the number of PA or DMA molecules. In the PA– NH_3 cluster system (Fig. S1), NH_3
148 accepts hydrogen atoms from the hydroxyl group in PA to generate NH_4^+ and ClO_4^- . It
149 should be noted that when the number of PA molecules is greater than or equal to the
150 number of NH_3 molecules, all NH_3 will be fully protonated. Similar to the PA–DMA
151 cluster system, halogen bonds do not appear in the PA– NH_3 cluster system. The
152 nitrogen atom of NH_3 and the hydrogen atom of the hydroxyl group in PA combine to



153 form the N–H...Cl–O hydrogen bond. However, proton transfer does not take place in
154 any of the PA–SA heteromolecular clusters (Fig. S10). Thus, hydrogen bonds (P–
155 O...H–O and O–H...O–S) and electrostatic interactions sustain the PA–SA cluster
156 system.

157 The ΔG values of $(PA)_{1-4}(DMA)_{1-4}$, $(PA)_{1-4}(NH_3)_{1-4}$ and $(PA)_{1-4}(SA)_{1-4}$ clusters
158 at the DLPNO-CCSD(T)/aug-cc-pVTZ// ω B97X-D/6-31++G(d,p) level of 278K, are
159 shown in Figure 2. The ΔG values of $(PA)_2$, $(PA)_3$ and $(PA)_4$ clusters are -0.06 , -0.99
160 and 2.90 kcal mol⁻¹, respectively, indicating that pure PA molecules are
161 thermodynamically less susceptible to forming clusters. The PA–DMA cluster growth
162 is more thermodynamically advantageous than the PA–NH₃ cluster growth, as
163 indicated by the fact that all ΔG values of the PA–DMA cluster system are lower than
164 those of the PA–NH₃ cluster system. Furthermore, the negative correlation between
165 temperature and the ΔG values of PA–DMA clusters is discovered (Figure S7, S8 and
166 S9), suggesting that the stability of PA–DMA clusters diminishes as the temperature
167 rises. The $(PA)_{1-4}(DMA)_1$ clusters are 15.15 - 38.79 kcal mol⁻¹ lower than those of the
168 corresponding $(PA)_{1-4}$ clusters, which suggests the possibility of collisional growth of
169 DMA with $(PA)_{1-4}$ clusters. The $(PA)_1(DMA)_1$, $(PA)_1(NH_3)_1$, and $(PA)_1(SA)_1$ initial
170 clusters are quite significant in the corresponding cluster systems, with ΔG values of
171 -15.15 , -9.73 , and -4.08 kcal mol⁻¹, respectively. The $(PA)_4(DMA)_4$ cluster has the
172 lowest ΔG value, as low as -127.04 kcal mol⁻¹. The PA–SA cluster system exhibits
173 the greatest ΔG values among the PA–DMA, PA–NH₃, and PA–SA cluster systems,
174 suggesting that it is a thermodynamically challenging system. In conclusion, DMA



175 has greater potential for PA-driven nucleation than NH_3 and SA based on the
176 thermodynamic data.

177 3.2 Evaporation Rates and Cluster Stability

178 The stability of the PA–DMA, PA– NH_3 , and PA–SA cluster systems is further
179 assessed by calculating the evaporation rates at 278 K based on the determined ΔG
180 values. The evaporation rate of DMA-rich clusters is higher than that of PA-rich
181 clusters, as illustrated in Fig. 3, suggesting that clusters with a high percentage of PA
182 molecules are more stable. $(\text{PA})_1(\text{DMA})_1$, $(\text{PA})_2(\text{DMA})_2$, $(\text{PA})_3(\text{DMA})_3$, and
183 $(\text{PA})_4(\text{DMA})_4$ clusters are all highly stable, with evaporation rates of 8×10^{-2} , $4 \times$
184 10^{-10} , 2×10^{-5} , and $4 \times 10^{-5} \text{ s}^{-1}$, respectively. All pure PA and DMA clusters are
185 unstable, with evaporation rates exceeding 10^9 s^{-1} . The PA–rich hetero molecular
186 clusters are more stable, probably because PA–rich clusters tend to contain more
187 hydrogen bonds and various intermolecular interactions.

188 With the exception of the $(\text{PA})_4(\text{DMA})_2$, $(\text{PA})_4(\text{DMA})_3$, and $(\text{PA})_4(\text{DMA})_4$
189 clusters, the evaporation rates of the majority of PA–DMA cluster systems are lower
190 than those of the comparable clusters of PA– NH_3 cluster systems. Similarly,
191 $(\text{PA})_1(\text{NH}_3)_1$, $(\text{PA})_2(\text{NH}_3)_2$, $(\text{PA})_3(\text{NH}_3)_3$, and $(\text{PA})_4(\text{NH}_3)_4$ clusters are the stable
192 clusters of the PA– NH_3 cluster system, which have evaporation rates of 3×10^{-2} , $2 \times$
193 10^{-1} , 3×10^0 , and $2 \times 10^{-8} \text{ s}^{-1}$, respectively. $(\text{PA})_1(\text{SA})_1$ cluster is the most stable
194 cluster with an evaporation rate as high as $6 \times 10^6 \text{ s}^{-1}$, suggesting the instability of
195 PA–SA clusters.

196 The actual Gibbs free energies of the PA–DMA systems affected by temperature



197 and vapor concentration were calculated, as shown in Figure. 4. At 278 K, for the
198 PA–DMA cluster system, $(PA)_1(DMA)_1$, $(PA)_2(DMA)_2$, $(PA)_3(DMA)_3$, and
199 $(PA)_4(DMA)_4$ clusters are the primary pathways and the growth process is unimpeded.
200 The decreasing trend of the actual Gibbs free energy during the formation of the
201 PA–DMA system is more pronounced with decreasing temperature, implying the
202 thermodynamic stability of the PA–DMA system.

203

204 3.3 Steady-State Cluster Concentrations and Nucleation Rate

205 To further assess the enhancement potential of DMA and NH_3 for PA-driven
206 nucleation, the simulated steady-state PA dimer concentration ($\sum[(PA)_2]$ (cm^{-3})) (a)
207 and the simulated cluster formation rate of the system, J ($cm^{-3} s^{-1}$) (b), at 278 K as the
208 function of $[PA]$ are shown in Figure. 5. It can be seen that the values of $\sum[(PA)_2]$ and
209 J of the PA-DMA system gradually increase with the increase of $[PA]$ and $[DMA]$
210 under simulated conditions. However, the effects of $[PA]$ and $[DMA]$ on $\sum[(PA)_2]$ and
211 J values gradually diminish with the increase of $[PA]$ and $[DMA]$. In the PA-DMA
212 system, neither $\sum[(PA)_2]$ nor J values were saturated with respect to $[DMA]$ at $[DMA]$
213 = 0.1 - 10 ppt and $[PA] = 10^6 - 10^8 cm^{-3}$. J values for the PA-DMA system were 10^{-1}
214 $cm^{-3} s^{-1}$ at 278 K, $[DMA] = 1$ ppt and $[PA] = 10^6 cm^{-3}$. Comparison of the cluster
215 formation rates, J ($cm^{-3} s^{-1}$), of PA-DMA and PA- NH_3 systems at 278 K; $[PA] = 10^6$
216 $-10^8 cm^{-3}$; $[DMA] = 1$ ppt; $[NH_3] = 100$ ppt; $CS = 2 \times 10^{-3} s^{-1}$, as shown in Fig. 5(c).
217 Even the concentrations of NH_3 are 2 orders of magnitude higher than those of the
218 DMA concentration, the J values of the PA–DMA cluster system are 8-10 orders of



219 magnitude higher than those of the PA–NH₃ cluster system for NH₃ concentrations
220 that are 2 orders of magnitude higher than those of the DMA concentration.

221 In addition, the trends of J for the PA–DMA cluster system at temperature of 238,
222 258 and 298 K; [PA] ($10^6 - 10^8 \text{ cm}^{-3}$) and [DMA] (0.1, 1 and 10 ppt) are shown in Fig.
223 6. As the temperature decreases (from 298 K to 258 K), the J value of the PA–DMA
224 cluster system increases. When the temperature range is 238–258 K, the J value of
225 PA–DMA cluster system tends to be saturated and does not change significantly with
226 temperature. The J value of the PA–DMA system is $1.65 \text{ cm}^{-3} \text{ s}^{-1}$ at 258 K, [DMA]=1
227 ppt and [PA]= 10^6 cm^{-3} .

228

229 3.4 Cluster Growth Route

230 The growth routes of the PA–DMA (a) and PA–NH₃ (b) systems at 278 K, [PA] = 10^6
231 cm^{-3} , [DMA] = 3 ppt, and [NH₃] = 100 ppt are shown in Fig. 6. The evaporation rates
232 of (PA)₂ and (DMA)₂ clusters are 4×10^9 and $2 \times 10^{12} \text{ s}^{-1}$. The higher evaporation rate
233 causes the PA–DMA system to form via the (PA)₁(DMA)₁ dimer pathway rather than
234 via the (PA)₂ and (DMA)₂ cluster pathways. The formation of the (PA)₁(DMA)₁ dimer
235 is the initial stage in the PA–DMA system. There is no branching during the growth of
236 clusters of the PA–DMA system, which may be due to the fact that the evaporation
237 rate of clusters on the diagonal (the number of PA molecules is the same as the
238 number of DMA molecules) is much lower than that of clusters off the diagonal (the
239 number of PA molecules is different from the number of DMA molecules). A
240 (PA)₂(DMA)₂ cluster complex is then formed by the combination of two



241 $(PA)_1(DMA)_1$ dimer clusters.

242 $(PA)_2(DMA)_2$ also has only one growth path and further collides with
243 $(PA)_1(DMA)_1$ to form a $(PA)_3(DMA)_3$ cluster. Eventually $(PA)_5(DMA)_4$ and
244 $(PA)_5(DMA)_5$ clusters are stable enough to grow from the PA-DMA system.
245 Therefore, collision between clusters with PA and DMA monomers is not the main
246 way in the PA-DMA cluster system. Cluster coalescence between a large number of
247 $(PA)_1(DMA)_1$ clusters play an important role in the growth of PA-DMA clusters,
248 which may be due to the low evaporation rate and high stability of $(PA)_1(DMA)_1$,
249 $(PA)_2(DMA)_2$, $(PA)_3(DMA)_3$, and $(PA)_4(DMA)_4$ clusters. The growth path of the
250 PA-NH₃ cluster system is very similar to that of the PA-DMA cluster system, in
251 which a PA monomer molecule collides with an NH₃ molecule to form a $(PA)_1(NH_3)_1$
252 dimer cluster, and then $(PA)_1(NH_3)_1$ dimer clusters are continuously added to form
253 $(PA)_4(NH_3)_4$ cluster.

254

255 **4 Atmospheric Implications and Conclusion**

256

257 In this paper, quantum chemical methods are used to study the energy minimum
258 configurations for the formation of atmospheric clusters of PA with DMA, NH₃ and
259 SA in the Arctic boundary layer. The evaporation rates, cluster formation rates and
260 growth paths of the nucleation process of PA with DMA, NH₃ and SA clusters are
261 simulated by inputting ACDC from the thermodynamic data obtained. The following
262 conclusions were drawn:



263 (1) Based on the Gibbs free energies calculated in this study, DMA and NH₃ can
264 strongly interact with PA through hydrogen bonding and proton transfer, thus
265 promoting the rapid formation of PA-DMA and PA-NH₃ clusters. No halogen bonds
266 are found in PA-DMA and PA-NH₃ clusters.

267 (2) Under the condition that the DMA concentration is two orders of magnitude
268 lower than the NH₃ concentration, the formation rate of PA-DMA clusters is much
269 faster than that of PA-NH₃ clusters. The cluster formation rate of the PA-SA cluster
270 system is the slowest among the three systems. This may be due to the fact that no
271 proton transfer occurs between the PA and SA molecules and only hydrogen bonding
272 stabilizes the clusters.

273 (3) The formation rate of pure PA clusters is extremely low. DMA can promote
274 the formation rate of PA clusters to a high level, which reflects the stabilizing effect of
275 DMA on PA clusters. The results suggest that PA can contribute to new particle
276 formation in the Arctic. The formation of (PA)₁(DMA)₁ and (PA)₁(NH₃)₁ dimers are
277 the decisive clusters for the growth of PA-DMA and PA-NH₃ cluster systems.

278 (4) PA can form stable binary clusters with DMA, which is an important step in
279 the formation of new particles in the atmosphere. The nucleation mechanism of
280 PA-DMA revealed in this study may contribute to a deeper understanding of the role
281 of marine chlorine-containing components on marine NPF.

282 Previous views hold that nucleation involving sulfuric acid/iodine oxoacid and
283 amines/ammonia is a key pathway for new particle formation in the polluted boundary
284 layer. This study extends this paradigm to a overlooked ocean-derived chlorinated



285 precursor: perchloric acid. The results of this study provide a partial explanation for
286 the “fate” of PA in the Arctic atmosphere: PA can not only be removed via wet and
287 dry deposition but is also likely to participate in new particle formation by reacting
288 with basic gases (especially DMA) to form stable clusters. This provides a theoretical
289 basis for understanding the role of chlorine-containing components, particularly
290 previously overlooked chlorate, in tropospheric aerosol nucleation.

291 This study indicates that perchloric acid has potential in new particle formation
292 in the Arctic marine boundary layer, particularly in the presence of dimethylamine.
293 This finding has significant atmospheric and climatic implications: first, it reveals a
294 potential new and efficient nucleation pathway between active chlorine released from
295 the ocean (via the formation of HClO_4) and nitrogen-containing bases (such as DMA
296 from marine biogenic sources), which may have important implications for assessing
297 the number of cloud condensation nuclei and cloud radiative forcing in the marine
298 boundary layer. Second, it expands our understanding of the atmospheric chlorine
299 cycle, indicating that, in addition to known deposition processes, gas-to-particle
300 transformations involving basic gases represent an important, previously
301 unrecognized atmospheric “sink” for HClO_4 . Therefore, future global and regional
302 climate models should incorporate HClO_4 and its nucleation mechanisms with amine
303 compounds when simulating aerosol formation over polar and marine regions, in
304 order to more accurately characterize aerosol-cloud-climate interactions.

305

306 **Data availability**



307

308 All data supported the paper are available from the article, supplementary information,
309 and the corresponding author upon reasonable request.

310

311 **Author Contributions Statement**

312 **Shengming Wang:** Investigation, Conceptualization, Formal analysis, Data curation,
313 Writing-original draft. **Xiangli Shi:** Methodology, Writing-reviewing and editing,
314 Validation, Supervision. **Qingzhu Zhang:** Methodology, Validation, Supervision,
315 Funding acquisition. **Wenxing Wang:** Resources, Funding acquisition,
316 Writing-reviewing and editing Supervision.

317

318 **Acknowledgements**

319

320 The work was financially supported by National Natural Science Foundation of China
321 (project No. 22236004, 21976107, 42075106, 42175122, 4217050207) and Taishan
322 Scholar Foundation of Shandong Province (No. ts201712003).

323

324

325 **Additional information**

326

327 **Competing interests:** The authors declare no competing financial interests.

328



329

References

330

- 331 Almeida, J., Schobesberger, S., Kürten, A., Ortega, I. K., Kupiainen-Määttä, O., Praplan, A. P., Adamov,
332 A., Amorim, A., Bianchi, F., and Breitenlechner, M.: Molecular understanding of sulphuric acid–amine
333 particle nucleation in the atmosphere, *Nature*, 502, 359-363, 2013.
- 334 Barrie, L., Bottenheim, J., Schnell, R. C., Crutzen, P., and Rasmussen, R.: Ozone destruction and
335 photochemical reactions at polar sunrise in the lower Arctic atmosphere, *Nature*, 334, 138-141, 1988.
- 336 Chen, M., Titcombe, M., Jiang, J., Jen, C., Kuang, C., Fischer, M. L., Eisele, F. L., Siepmann, J. I.,
337 Hanson, D. R., and Zhao, J.: Acid–base chemical reaction model for nucleation rates in the polluted
338 atmospheric boundary layer, *Proceedings of the National Academy of Sciences*, 109, 18713-18718,
339 2012.
- 340 Chu, B., Kerminen, V.-M., Bianchi, F., Yan, C., Petäjä, T., and Kulmala, M.: Atmospheric new particle
341 formation in China, *Atmospheric Chemistry and Physics*, 19, 115-138, 2019.
- 342 Dasgupta, P. K., Martinelango, P. K., Jackson, W. A., Anderson, T. A., Tian, K., Tock, R. W., and
343 Rajagopalan, S.: The origin of naturally occurring perchlorate: the role of atmospheric processes,
344 *Environ. Sci. Technol.*, 39, 1569-1575, 2005.
- 345 Ehn, M., Thornton, J. A., Kleist, E., Sipilä, M., Junninen, H., Pullinen, I., Springer, M., Rubach, F.,
346 Tillmann, R., and Lee, B.: A large source of low-volatility secondary organic aerosol, *Nature*, 506,
347 476-479, 2014.
- 348 Erupe, M., Viggiano, A., and Lee, S.-H.: The effect of trimethylamine on atmospheric nucleation
349 involving H₂SO₄, *Atmospheric Chemistry and Physics*, 11, 4767-4775, 2011.
- 350 Frisch, M., Trucks, G., Schlegel, H., Scuseria, G., Robb, M., Cheeseman, J., Scalmani, G., Barone, V.,
351 Petersson, G., and Nakatsuji, H.: Gaussian 16, Revision A. 03, Gaussian, Inc., Wallingford CT, 3, 2016.
- 352 Furdui, V. I. and Tomassini, F.: Trends and sources of perchlorate in Arctic snow, *Environmental
353 science & technology*, 44, 588-592, 2010.
- 354 Ge, X., Wexler, A. S., and Clegg, S. L.: Atmospheric amines—Part II. Thermodynamic properties and
355 gas/particle partitioning, *Atmos. Environ.*, 45, 561-577, 2011.
- 356 Jaeglé, L., Yung, Y. L., Toon, G. C., Sen, B., and Blavier, J. F.: Balloon observations of organic and
357 inorganic chlorine in the stratosphere: The role of HClO₄ production on sulfate aerosols, *Geophysical
358 research letters*, 23, 1749-1752, 1996.
- 359 Jen, C. N., McMurry, P. H., and Hanson, D. R.: Stabilization of sulfuric acid dimers by ammonia,
360 methylamine, dimethylamine, and trimethylamine, *Journal of Geophysical Research: Atmospheres*, 119,
361 7502-7514, 2014.
- 362 Kalivitis, N., Kerminen, V.-M., Kouvarakis, G., Stavroulas, I., Tzitzikalaki, E., Kalkavouras, P.,
363 Daskalakis, N., Myriokefalitakis, S., Bougiatioti, A., and Manninen, H. E.: Formation and growth of
364 atmospheric nanoparticles in the eastern Mediterranean: results from long-term measurements and
365 process simulations, *Atmospheric Chemistry and Physics*, 19, 2671-2686, 2019.
- 366 Karaboga, D.: An idea based on honey bee swarm for numerical optimization, 2005.
- 367 Lee, S. H., Gordon, H., Yu, H., Lehtipalo, K., Haley, R., Li, Y., and Zhang, R.: New particle formation
368 in the atmosphere: From molecular clusters to global climate, *Journal of Geophysical Research:
369 Atmospheres*, 124, 7098-7146, 2019.
- 370 Loukonen, V., Kurtén, T., Ortega, I., Vehkamäki, H., Padua, A. A., Sellegri, K., and Kulmala, M.:



- 371 Enhancing effect of dimethylamine in sulfuric acid nucleation in the presence of water—a computational
372 study, *Atmospheric Chemistry and Physics*, 10, 4961-4974, 2010.
- 373 Masson-Delmotte, V., Zhai, P., Pirani, S., Connors, C., Péan, S., Berger, N., Caud, Y., Chen, L.,
374 Goldfarb, M., and Scheel Monteiro, P. M.: *Ipc*, 2021: Summary for policymakers. in: *Climate change*
375 2021: The physical science basis. contribution of working group i to the sixth assessment report of the
376 intergovernmental panel on climate change, 2021.
- 377 McGrath, M., Olenius, T., Ortega, I., Loukonen, V., Paasonen, P., Kurtén, T., Kulmala, M., and
378 Vehkamäki, H.: Atmospheric Cluster Dynamics Code: a flexible method for solution of the birth-death
379 equations, *Atmospheric Chemistry and Physics*, 12, 2345-2355, 2012a.
- 380 McGrath, M. J., Olenius, T., Ortega, I., Loukonen, V., Paasonen, P., Kurtén, T., Kulmala, M., and
381 Vehkamäki, H.: Atmospheric Cluster Dynamics Code: a flexible method for solution of the birth-death
382 equations, *Atmospheric Chemistry and Physics*, 12, 2345-2355, 2012b.
- 383 Neese, F.: The ORCA program system, *Wiley Interdisciplinary Reviews: Computational Molecular*
384 *Science*, 2, 73-78, 2012.
- 385 Rajagopalan, S., Anderson, T., Cox, S., Harvey, G., Cheng, Q., and Jackson, W. A.: Perchlorate in wet
386 deposition across North America, *Environ. Sci. Technol.*, 43, 616-622, 2009.
- 387 Rappé, A. K., Casewit, C. J., Colwell, K. S., Goddard III, W. A., and Skiff, W. M.: UFF, a full periodic
388 table force field for molecular mechanics and molecular dynamics simulations, *Journal of the American*
389 *chemical society*, 114, 10024-10035, 1992.
- 390 Sander, S. P., Friedl, R. R., and Yung, Y. L.: Rate of formation of the ClO dimer in the polar
391 stratosphere: Implications for ozone loss, *Science*, 245, 1095-1098, 1989.
- 392 Tham, Y. J., Sarnela, N., Iyer, S., Li, Q., Angot, H., Quéléver, L. L., Beck, I., Laurila, T., Beck, L. J.,
393 and Boyer, M.: Widespread detection of chlorine oxyacids in the Arctic atmosphere, *Nature*
394 *Communications*, 14, 1769, 2023.
- 395 Wang, S., Zhang, H., Shi, X., Zhang, Q., Wang, W., and Wang, Q.: Chloric acid-driven nucleation
396 enhanced by dimethylamine and sulfuric acid in the Arctic: mechanistic study, *Atmospheric Chemistry*
397 *and Physics*, 25, 15359-15368, 2025.
- 398 Webster, C., May, R., Toohey, D., Avallone, L., Anderson, J., Newman, P., Lait, L., Schoeberl, M.,
399 Elkins, J., and Chan, K.: Chlorine chemistry on polar stratospheric cloud particles in the Arctic winter,
400 *Science*, 261, 1130-1134, 1993.
- 401 Xie, H.-B., Elm, J., Halonen, R., Myllys, N., Kurten, T., Kulmala, M., and Vehkamäki, H.: Atmospheric
402 fate of monoethanolamine: enhancing new particle formation of sulfuric acid as an important removal
403 process, *Environmental science & technology*, 51, 8422-8431, 2017.
- 404 Zhang, J. and Dolg, M.: ABCluster: the artificial bee colony algorithm for cluster global optimization,
405 *Physical Chemistry Chemical Physics*, 17, 24173-24181, 2015.
- 406 Zhang, R.: Getting to the critical nucleus of aerosol formation, *Science*, 328, 1366-1367, 2010.
- 407 Zhao, J., Eisele, F. L., Titcombe, M., Kuang, C., and McMurry, P. H.: Chemical ionization mass
408 spectrometric measurements of atmospheric neutral clusters using the cluster - CIMS, *Journal of*
409 *Geophysical Research: Atmospheres*, 115, 2010.
- 410 Zollner, J., Glasoe, W., Panta, B., Carlson, K., McMurry, P., and Hanson, D.: Sulfuric acid nucleation:
411 power dependencies, variation with relative humidity, and effect of bases, *Atmospheric Chemistry and*
412 *Physics*, 12, 4399-4411, 2012.

413

414



415

Figure Captions

416

417 **Figure 1.** Identified minimum free energy configurations of the $(\text{PA})_{1-4}(\text{DMA})_{1-4}$
418 clusters at the DLPNO-CCSD(T)/aug-cc-pVTZ// ω B97X-D/6-31++G(d,p) level of
419 theory. The atoms of oxygen, nitrogen, chlorine, carbon, and hydrogen are
420 represented by the red, blue, green, gray, and white balls, respectively. Hydrogen
421 bonds are indicated by the dashed white lines.

422

423 **Figure 2.** At the DLPNO-CCSD(T)/aug-cc-pVTZ// ω B97X-D/6-31++G(d,p) level of
424 theory, the formation free energy (ΔG) (in kcal mol⁻¹) of (a) $(\text{PA})_{1-4}(\text{DMA})_{1-4}$, (b)
425 $(\text{PA})_{1-4}(\text{NH}_3)_{1-4}$ and (c) $(\text{PA})_{1-4}(\text{SA})_{1-4}$ clusters. The computations are carried out at 1
426 atm and 278 K.

427

428 **Figure 3.** Evaporation rates for (a) $(\text{PA})_{1-4}(\text{DMA})_{1-4}$ and (b) $(\text{PA})_{1-4}(\text{NH}_3)_{1-4}$ (c)
429 $(\text{PA})_{1-4}(\text{SA})_{1-4}$ clusters at 278 K and 1 atm.

430

431 **Figure 4.** Actual Gibbs free energy of the PA-DMA clusters at 278, 258 and 238K.

432

433 **Figure 5.** Simulated steady-state PA dimer concentration $\Sigma[(\text{PA})_2]$ (cm⁻³) (a) and the
434 cluster formation rates J (cm⁻³ s⁻¹) of the simulation systems (b) as a function of $[\text{PA}]$
435 at 278 K. (c) Comparison of the cluster formation rates J (cm⁻³ s⁻¹) of PA-DMA
436 clusters with PA-NH₃ clusters at 278 K; $[\text{PA}] = 10^6 - 10^8$ cm⁻³; $[\text{DMA}] = 1$ ppt; $[\text{NH}_3]$



437 = 100 ppt; and $CS = 2 \times 10^{-3} \text{ s}^{-1}$. The ΔG values at the
438 DLPNO-CCSD(T)/aug-cc-pVTZ// ω B97X-D/6-31++G(d,p) level are used to compute
439 the PA–DMA and PA–NH₃ rates.

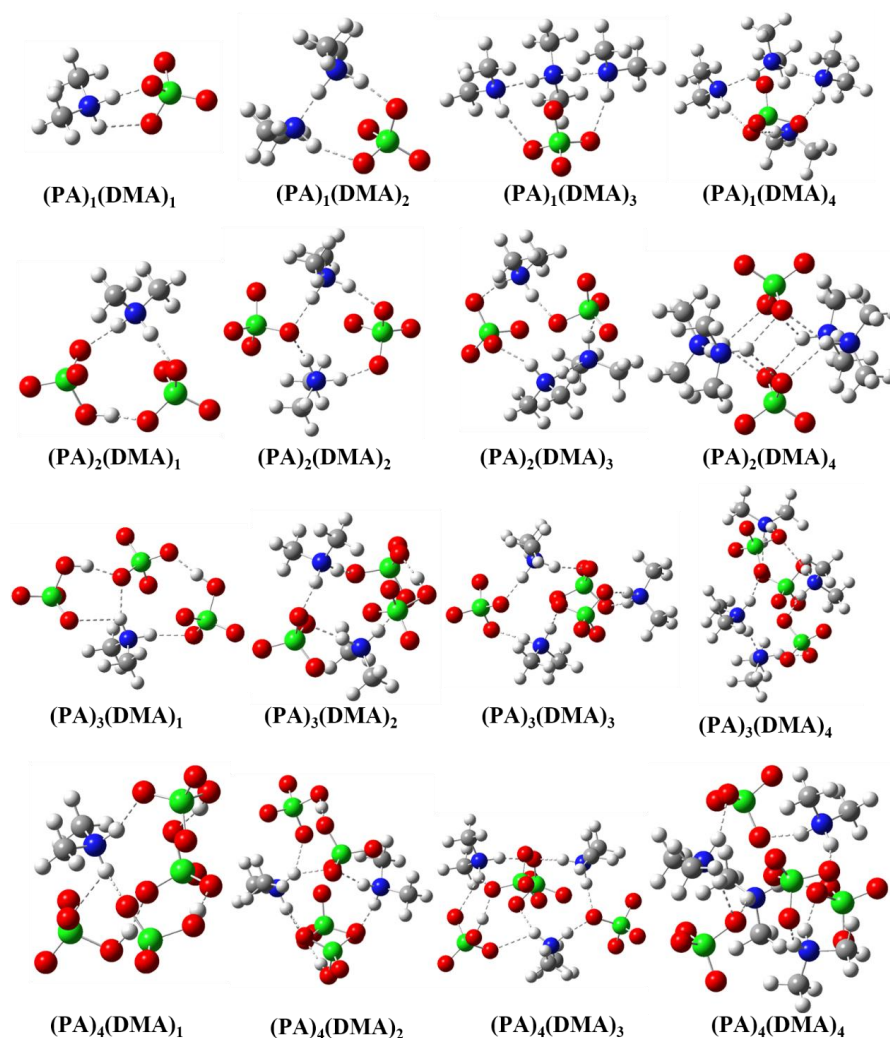
440

441 **Figure 6.** The simulated cluster formation rate J ($\text{cm}^{-3} \text{ s}^{-1}$) of the PA-DMA system at
442 different temperatures (A) 238, (B) 258 K, and (C) 298 K; $[PA] = 10^6 - 10^8 \text{ molec.}$
443 cm^{-3} ; $[DMA] = 0.1, 1, \text{ and } 10 \text{ ppt}$; and $CS = 2 \times 10^{-3} \text{ s}^{-1}$.

444

445 **Figure 7.** (a) Main clustering routes of $(PA)_{1-4}(DMA)_{1-4}$ clusters at 278 K, $[PA] = 10^6$
446 cm^{-3} , and $[DMA] = 3 \text{ ppt}$. (b) Main clustering routes of $(PA)_{1-4}(\text{NH}_3)_{1-4}$ clusters at
447 278 K, $[PA] = 10^6 \text{ cm}^{-3}$, and $[\text{NH}_3] = 100 \text{ ppt}$.

448



449

450 **Figure 1.** Identified minimum free energy configurations of the (PA)₁₋₄(DMA)₁₋₄

451 clusters at the DLPNO-CCSD(T)/aug-cc-pVTZ// ω B97X-D/6-31++G(d,p) level of

452 theory. The atoms of oxygen, nitrogen, chlorine, carbon, and hydrogen are

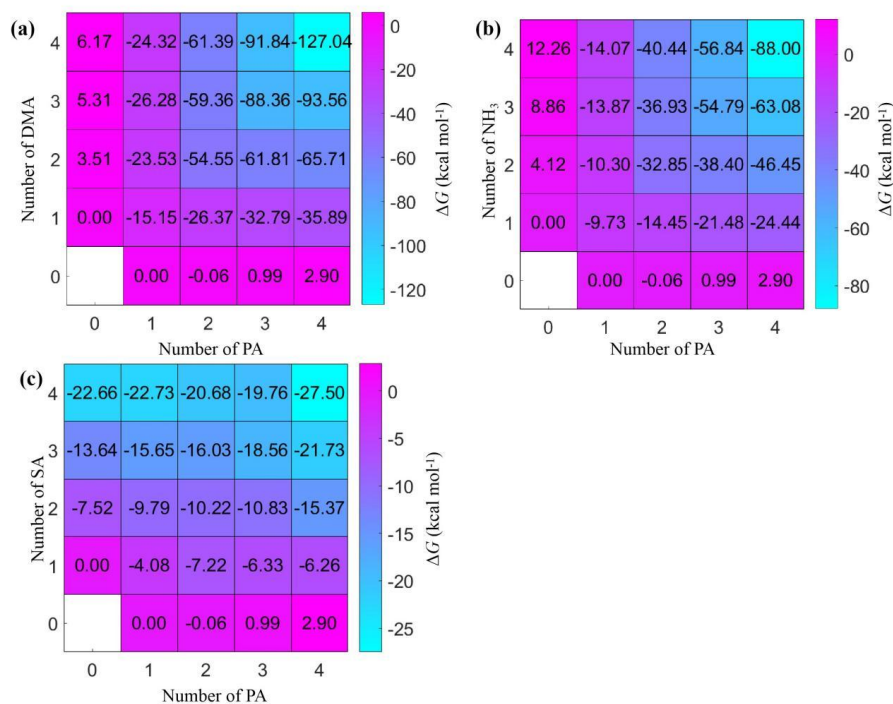
453 represented by the red, blue, green, gray, and white balls, respectively. Hydrogen

454 bonds are indicated by the dashed white lines.

455



456



457

458 **Figure 2.** At the DLPNO-CCSD(T)/aug-cc-pVTZ// ω B97X-D/6-31++G(d,p) level of

459 theory, the formation free energy (ΔG) (in kcal mol⁻¹) of (a) $(\text{PA})_{1-4}(\text{DMA})_{1-4}$, (b)

460 $(\text{PA})_{1-4}(\text{NH}_3)_{1-4}$ and (c) $(\text{PA})_{1-4}(\text{SA})_{1-4}$ clusters. The computations are carried out at 1

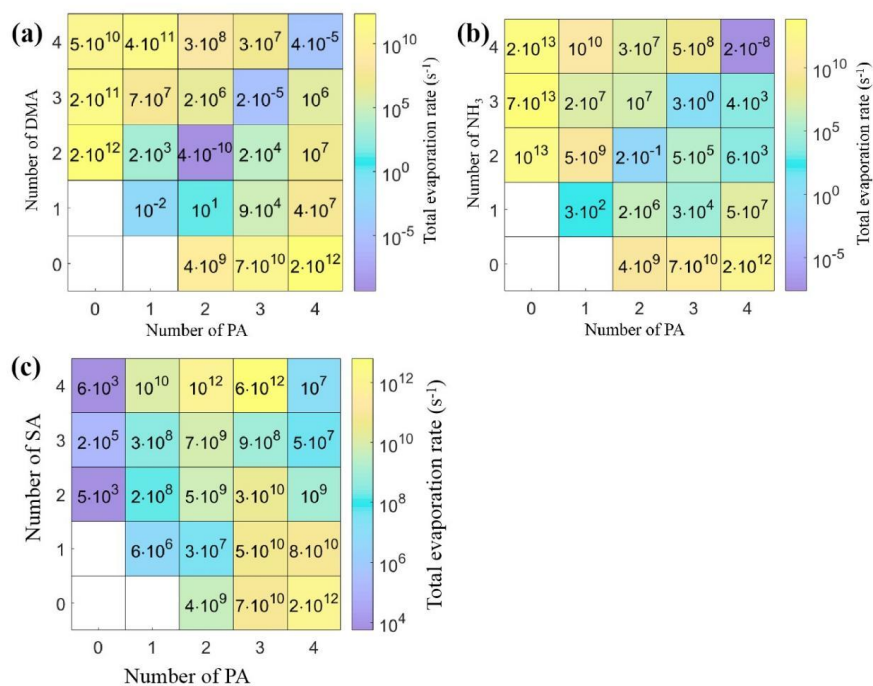
461 atm and 278 K.

462

463

464

465



466

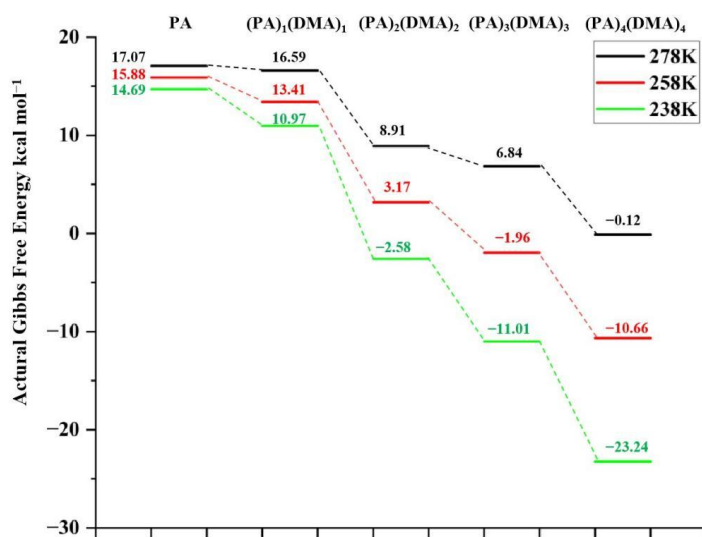
467 **Figure 3.** Evaporation rates for (a) (PA)₁₋₄(DMA)₁₋₄ and (b) (PA)₁₋₄(NH₃)₁₋₄ (c)

468 (PA)₁₋₄(SA)₁₋₄ clusters at 278 K and 1 am.

469

470

471



472

473 **Figure 4.** Actual Gibbs free energy of the PA-DMA clusters at 278, 258 and 238K.

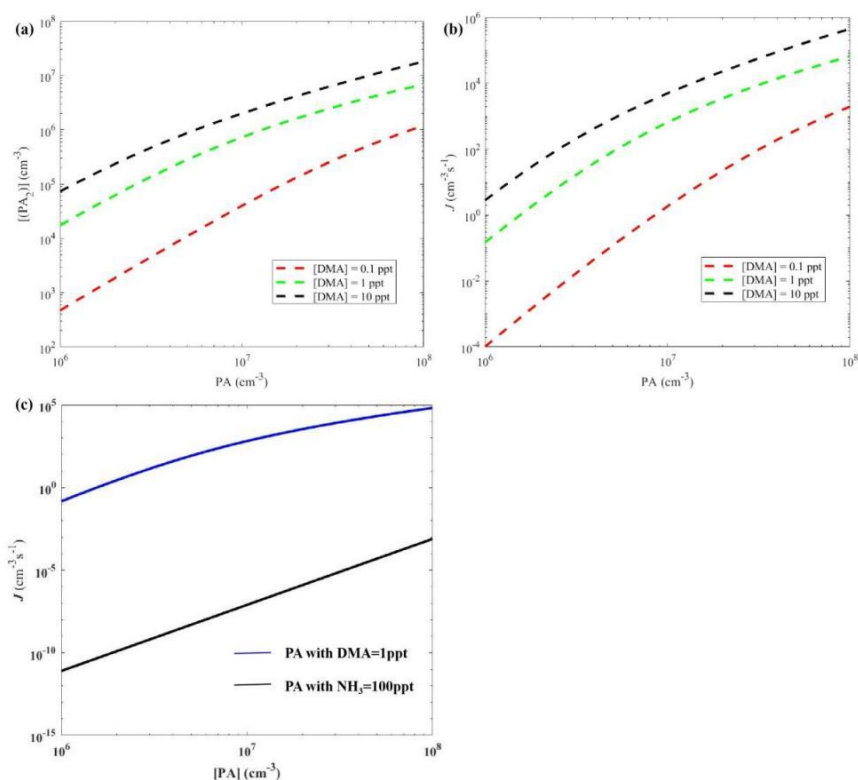
474

475

476

477

478



479

480 **Figure 5.** Simulated steady-state PA dimer concentration $\Sigma[(PA)_2]$ (cm^{-3}) (a) and the

481 cluster formation rates J ($cm^{-3} s^{-1}$) of the simulation systems (b) as a function of $[PA]$

482 at 278 K. (c) Comparison of the cluster formation rates J ($cm^{-3} s^{-1}$) of PA–DMA

483 clusters with PA–NH₃ clusters at 278 K; $[PA] = 10^6 - 10^8 cm^{-3}$; $[DMA] = 1 ppt$; $[NH_3]$

484 = 100 ppt; and $CS = 2 \times 10^{-3} s^{-1}$. The ΔG values at the

485 DLPNO-CCSD(T)/aug-cc-pVTZ// ω B97X-D/6-31++G(d,p) level are used to compute

486 the PA–DMA and PA–NH₃ rates.

487

488

489



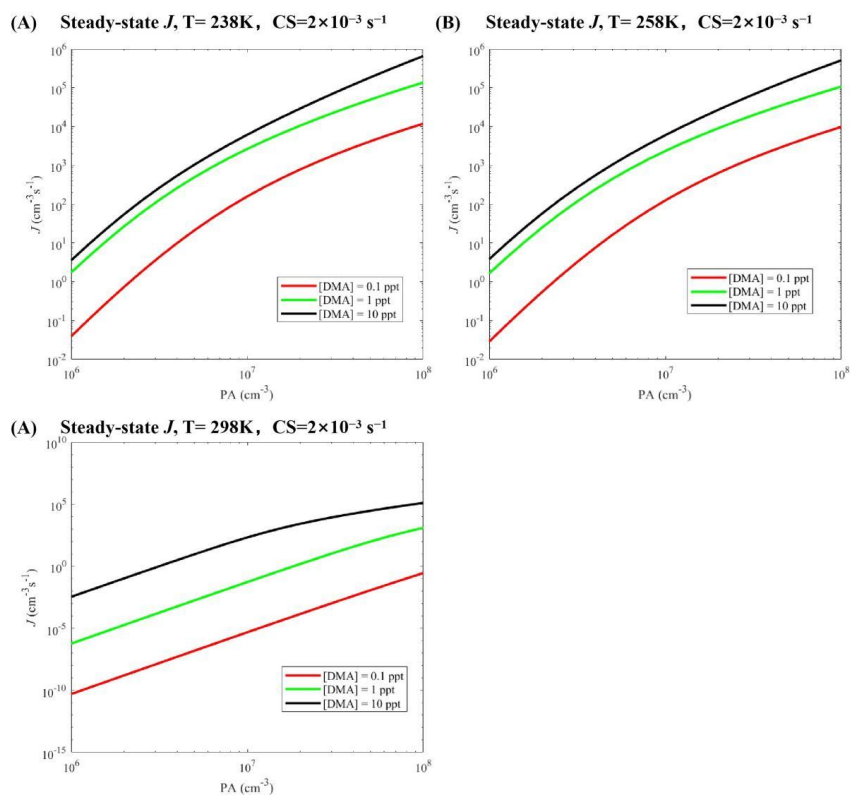
490

491

492

493

494



495

496 **Figure 6.** The simulated cluster formation rate J ($\text{cm}^{-3}\text{ s}^{-1}$) of the PA-DMA system at
497 different temperatures (A) 238, (B) 258 K, and (C) 298 K; $[\text{PA}] = 10^6 - 10^8$ molec.

498 cm^{-3} ; $[\text{DMA}] = 0.1, 1, \text{ and } 10$ ppt; and $CS = 2\times 10^{-3}\text{ s}^{-1}$.

499

500



501

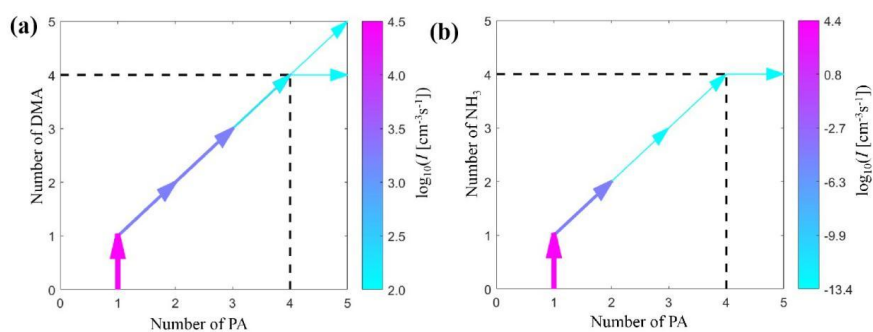
502

503

504

505

506



507

508

509 **Figure 7.** (a) Main clustering routes of $(PA)_{1-4}(DMA)_{1-4}$ clusters at 278 K, $[PA] = 10^6$

510 cm^{-3} , and $[DMA] = 3$ ppt. (b) Main clustering routes of $(PA)_{1-4}(NH_3)_{1-4}$ clusters at

511 278 K, $[PA] = 10^6 cm^{-3}$, and $[NH_3] = 100$ ppt.

512

513

514

515

516

517

518